Deep-Sea Research Part I 131 (2018) 93–100

Contents lists available at ScienceDirect

Deep-Sea Research Part I

journal homepage: www.elsevier.com/locate/dsri

Are deep-sea ecosystems surrounding Madagascar threatened by land-use or climate change?

Christophe Fontanier[a,b,c,d,*], Briony Mamo[e], Samuel Toucanne[c], Germain Bayon[c], Sabine Schmidt[b], Bruno Deflandre[b], Bernard Dennielou[c], Gwenael Jouet[c], Eline Garnier[a,c], Saburo Sakai[f], Ruth Martinez Lamas[c], Pauline Duros[b,c], Takashi Toyofuku[f], Aurélien Salé[c], Déborah Belleney[c], Sabrina Bichon[b], Audrey Boissier[c], Sandrine Chéron[c], Mathilde Pitel[c], Angélique Roubi[c], Mickaël Rovere[c], Antoine Grémare[b], Stéphanie Dupré[c], Stéphan J. Jorry[c]

[a] Univ. Bordeaux, CNRS, Environnements et Paléo-environnements Océaniques et Continentaux, UMR 5805, F-33600 Pessac, France
[b] FORAM, Research Group, F-49140 Villevêque, France
[c] Ifremer, Unité Géosciences Marines, Centre de Brest, BP 70, F-29280 Plouzané, France
[d] Univ. Angers, F49035 Angers, France
[e] The University of Hong Kong, Department of Biological Sciences, Pokfulam Road, Hong Kong SAR
[f] Japan Agency for Marine-Earth Science and Technology (JAMSTEC), Institute of Biogeosciences, 2-15 Natsushima-cho, Yokosuka 237-0061, Japan

ARTICLE INFO

Keywords:
Multidisciplinary study
Benthic foraminifera
Land-use
Tropical cyclones

ABSTRACT

In this short communication, we present a multidisciplinary study of sedimentary records collected from a deep-sea interfluve proximal to the mouths of major northwestern Madagascan rivers. For the last 60 years, the seafloor has been repeatedly disturbed by the deposition of organic rich, tropical, terrestrial sediments causing marked reductions in benthic biodiversity. Increased soil erosion due to local land-use, deforestation and intensifying tropical cyclones are potential causes for this sedimentary budget and biodiversity shift. Our marine sedimentary records indicate that until now, these conditions have not occurred within the region for at least 20,000 years.

1. Introduction

The rich ecosystem of Madagascar, one of Earth's biodiversity hotspots, is endangered due to historical changes in land-use and related deforestation (Green and Sussman, 1990; Gade, 1996; Myers et al., 2000; Harper et al., 2007; Waeber et al., 2015). The clearing of tropical forests for extensive logging and agricultural exploitation by early 20th century colonies (Jarosz, 1993) is considered to have exacerbated soil erosion during torrential rains (e.g., Saboureau, 1959; Gade, 1996). That being said, the exclusive causality between anthropogenic land-use and increased erosion has been thoroughly debated for the last two decades (Kull, 2000; Klein, 2002). Erosional gullies (i.e. lavakas) are more abundant in seismically active areas, which suggests a complex relationship between tectonics and regional erosional processes (Cox et al., 2010). During rainy seasons, weathered red lateritic soils are washed into rivers which then drain into coastal watersheds. From space, astronauts describe Madagascar as 'bleeding into the ocean' (Fig. 1) (Helfert and Wood, 1986).

Despite identifying the impact of modern, human-induced deforestation and subsequent soil erosion on coral reefs (Maina et al., 2013; Grove et al., 2013), no investigation has ever assessed the potential and combined impact of modern land-use and extreme meteorological events (i.e., tropical cyclones) on deep-sea ecosystems. To further explore these issues, we analysed marine sediment cores recovered from ~ 780 m depth in the Mozambique Channel, off the Betsiboka and Mahavavy Sud Rivers (Fig. 1). Both major rivers drain from the highlands of central Madagascar. Cores MOZ1-MTB6 and MOZ1-MTB7 (each 50 cm long) were recovered from a steep interfluve and provide a 1000-yr record of sediment discharge from northwest (NW) Madagascar (Fig. 1) (Olu, 2014). For comparison, an additional 10 m-core (MOZ1-KSF-10) was collected at the same location covering the last ~ 20,000 years.

2. Material and methods

Cores MOZ1-MTB-6 and MOZ1-MTB-7 were collected with a Barnett-type multi-corer equipped with 8 PCPE tubes (96 mm internal diameter). Core MOZ1-MTB-6 was dedicated to sedimentary organic

* Corresponding author at: Univ. Bordeaux, CNRS, Environnements et Paléo-environnements Océaniques et Continentaux, UMR 5805, F-33600 Pessac, France.
E-mail address: c.fontanier@foram.eu.com (C. Fontanier).

https://doi.org/10.1016/j.dsr.2017.11.011
Received 6 June 2017; Received in revised form 24 November 2017; Accepted 24 November 2017
Available online 05 December 2017
0967-0637/ © 2017 Elsevier Ltd. All rights reserved.

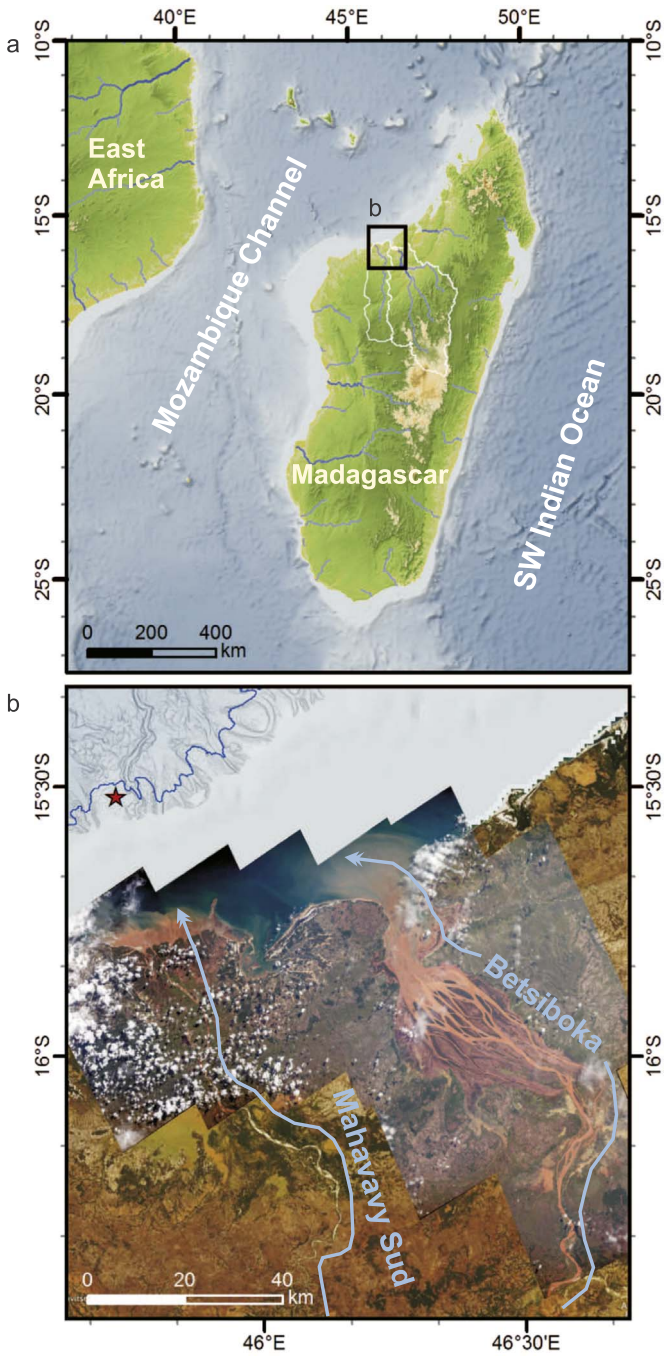

Fig. 1. Study area off NW Madagascar. a: General location of Madagascar. The Mahavavy Sud and Betsiboka watersheds are outlined in white and main Madagascan and East African rivers in blue. Bathymetry is extracted from Gebco (General Bathymetric Chart of the Oceans). River pathways are extracted from FAO archives. **b:** Location of multicorer deployments (MOZ1-MTB-6 and MOZ1-MTB-7) and MOZ1-KSF-10 core are indicated by the red star (− 15°31.15′ N; 45°42.94′ E; ~ 780 m; Olu, 2014). Bathymetry was mapped during the PTOLEMEE cruise using a EM302 multibeam echosounder (Jorry, 2014). The 1000-m isobath is outlined in dark blue. The paths of both Mahavay Sud and Betsiboka rivers were photographed from the International Space Station on March 21st, 2016. Image courtesy of the Earth Science and Remote Sensing Unit, NASA Johnson Space Center (http://eol.jsc.nasa.gov/Collections/Composites/). Terrestrial backgrounds were extracted from MapBox satellite data. Projection: World Mercator. Geodetic system: WGS84. (For interpretation of the references to color in this figure legend, the reader is referred to the web version of this article.)

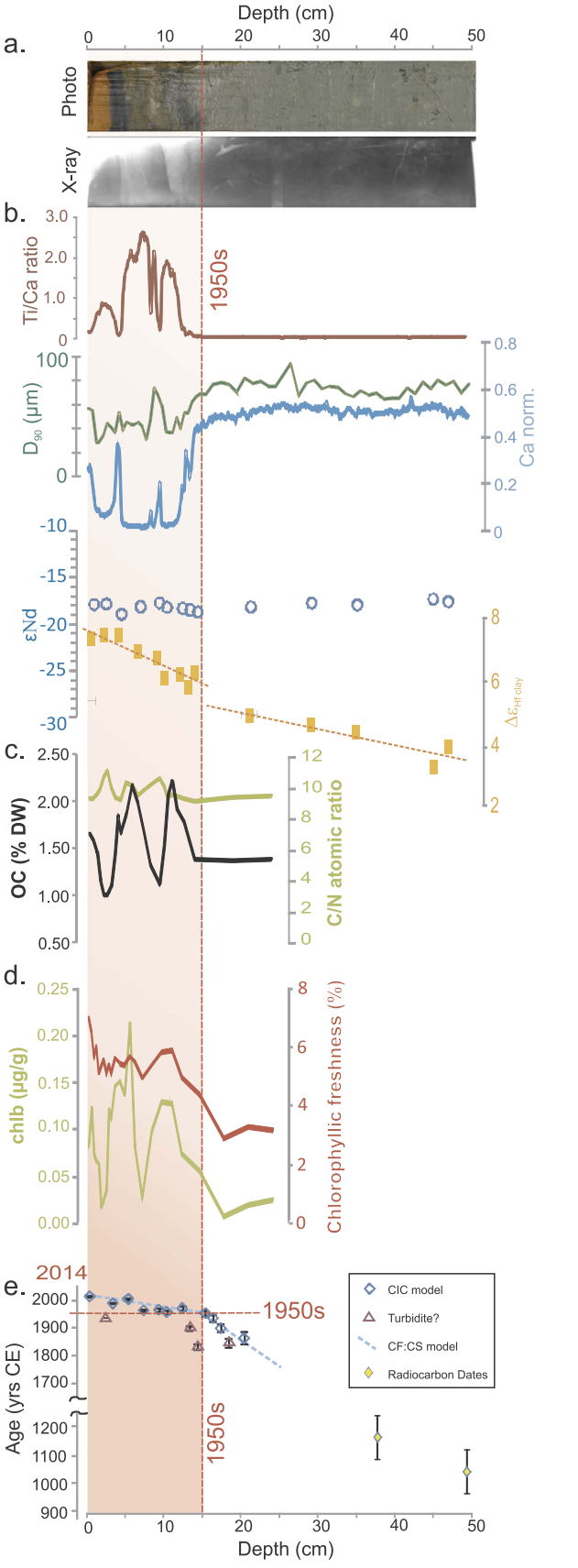

(caption on next page)

Fig. 2. Mass deposition of terrigenous sediments on the deep-sea since the 1950s. Sedimentological, geochemical and faunal properties of both cores MOZ1-MTB-6 and MOZ1-MTB-7. **a:** Photograph and X-ray radiography of core MOZ1-MTB-7. **b:** Ti/Ca ratio, Grain size, Ca normalised, ε_{Nd}, $\Delta\varepsilon_{Hf\ clay}$ in core MOZ1-MTB-7. **c:** Indicators of sedimentary organic matter (OC %DW, C/N atomic ratio) in core MOZ1-MTB-6. **d:** Chl *b* content (in µg/g) and Chlorophyll Freshness index (= [(Chl *a* + Chl *b*)/(Chl *a* + Chl *b* + Pheo *a* + Pheo *b*)] ratio in %) in core MOZ1-MTB-6. **e:** Age model of core MOZ1-MTB-7 based on total ^{210}Pb activity (blue diamonds) and radiocarbon dates (indicated by yellow diamonds). Pale red band indicates sediments deposited since the 1950s.

matter analysis and sliced horizontally. Core MOZ1-MTB7 was splitted longitudinally in half. One half was photographed then radiographed with a Geotek-MSCL-XCT (Fig. 2). Both halves were then used for other analyses. The kullenberg-type piston core MOZ1-KSF-10 was recovered within the same study area, a few meters away from MOZ1-MTB-6 (Olu, 2014).

2.1. X-ray fluorescence (XRF)

Semi-quantitative geochemical composition of bulk sediment was measured with an Avaatech X-ray fluorescence (XRF) core scanner on both cores MOZ1-MTB-7 and MOZ1-KSF-10.

2.2. Grain size analysis

Grain size analysis was carried out on core MOZ1-MTB-7 core with a Mastersizer 3000 laser diffraction particle size analyzer on the bulk sediment fraction. Sediment samples were taken every 0.5 cm in the uppermost 15 cm, then every 1 cm between 15 and 50 cm down core with a total of 65 samples analysed. Sample pre-treatment constituted taking small amounts of sediment (1 g), mixing them with distilled

Table 2
Sedimentary organic matter descriptors (OC %DW, C/N atomic ratio) in core MOZ1-MTB-6.

MOZ1-MTB-6			
Sediment interval (cm)	**OC (% DW)**	**C/N atomic ratio**	**$CaCO_3$ (% DW)**
0–0.5	3.5	9.2	15.2
0.5–1	3.3	9.2	14.7
1–1.5	2.8	9.5	11.1
1.5–2	2.1	9.8	7.4
2–2.5	1.5	10.6	3.9
2.5–3	1.5	11.1	4.4
3–3.5	1.9	9.9	7.2
3.5–4	2.7	9.3	10.4
4–4.5	3.1	9.2	10.5
4.5–5	2.1	9.1	3.7
5–6	1.9	10.2	0.3
6–7	2.4	10.1	1.6
7–8	2.4	9.4	3.1
8–9	2.0	9.7	2.6
9–10	1.8	10.1	4.1
10–12	2.3	10.5	9.8
12–14	2.4	10.0	7.3
14–16	2.7	9.3	5.6
16–18	2.6	9.5	3.2
18–20	3.2	9.4	11.0
20–25	4.1	9.2	19.2
25–30	5.9	9.0	37.6
30–35	5.5	9.4	34.8
35–40	5.6	9.4	35.3

Table 1
Grain size (D_{10}, D_{50} and D_{90} in µm) in core MOZ1-MTB-7.

MOZ1-MTB-7				MOZ1-MTB-7			
Sediment interval (cm)	**D_{10} (µm)**	**D_{50} (µm)**	**D_{90} (µm)**	**Sediment interval (cm)**	**D_{10} (µm)**	**D_{50} (µm)**	**D_{90} (µm)**
0–0.5	2	7	56	18–19	2	8	76
0.5–1	2	7	54	19–20	2	8	70
1–1.5	1	6	28	20–21	2	8	81
1.5–2	1	6	28	21–22	2	8	77
2–2.5	1	6	33	22–23	2	8	78
2.5–3	2	7	43	23–24	2	8	75
3–3.5	2	7	40	24–25	2	8	75
3.5–4	2	7	36	25–26	2	9	84
4–4.5	2	8	52	26–27	2	9	94
4.5–5	2	7	38	27–28	2	8	66
5–5.5	2	8	44	28–29	2	9	77
5.5–6	2	8	43	29–30	2	9	79
6–6.5	2	8	42	30–31	2	8	72
6.5–7	2	8	44	31–32	2	8	75
7–7.5	2	8	41	32–33	2	8	74
7.5–8	2	6	31	33–34	2	8	68
8–8.5	2	8	46	34–35	2	8	66
8.5–9	2	12	73	35–36	2	8	70
9–9.5	2	10	67	36–37	2	8	68
9.5–10	2	9	58	37–38	2	8	69
10–10.5	2	7	37	38–39	2	8	64
10.5–11	2	7	37	39–40	2	7	65
11–11.5	2	8	36	40–41	2	8	64
11.5–12	2	8	49	41–42	2	8	73
12–12.5	2	7	40	42–43	2	8	68
12.5–13	2	8	53	43–44	2	8	78
13–13.5	2	8	53	44–45	2	8	72
13.5–14	2	7	61	45–46	2	8	79
14–14.5	2	8	66	46–47	2	8	75
14.5–15	2	7	68	47–48	2	8	79
15–16	2	8	68	48–49	2	8	68
16–17	2	9	76	49–50	2	8	76
17–18	2	8	77				

water and agitating until there was a homogeneous mix (4–10 min). The 10th, 50th and 90th percentiles (D_{10}, D_{50} and D_{90}, respectively) were calculated for each sample (Table 1).

2.3. Organic matter

Detailed descriptions regarding sample preparation are published elsewhere (Fontanier et al., 2016). Total carbon (TC) and nitrogen (TN) contents were measured in triplicate on freeze-dried sediments by combustion using an automatic ThermoFinnigan EA1112 Series Flash Elemental analyzer (Table 2). Total Organic Carbon (OC) content was similarly measured after removal of carbonates with 2MHCl per sample and reproducibility was < 5%. C/N ratios (i.e. OC/TN) were expressed as atomic ratios (Pastor et al., 2011). For chloropigments, 0.5–3.7 g FW (Fresh Weight) of frozen (− 80 °C) sediment subsamples were extracted overnight at 4 °C in darkness in 5 mL of 90% acetone (final concentration taking into account the water content of sediments). Fluorescence measurements were then performed using a Perkin Elmer® LS55 spectrofluorometer (Neveux and Lantoine, 1993). This enabled for the assessment of chlorophyll *a* (Chl-*a*), chlorophyll *b* (Chl-*b*), pheophytin *a* (Phaeo-*a*) and pheophytin *b* (Phaeo-*b*). The [(Chl *a* + Chl *b*)/(Chl *a* + Chl *b* + Pheo *a* + Pheo *b*)] ratio (expressed in %) was computed to indicate the freshness of chlorophyll-related pigments.

2.4. Neodymium and Hafnium isotopes

Detailed descriptions regarding sample preparation are published elsewhere (Bayon et al., 2016). Neodymium and hafnium isotopic measurements were performed with a multi-collector ICPMS (Table 3). Mass bias corrections were made using $^{146}Nd/^{144}Nd = 0.7219$ and $^{179}Hf/^{177}Hf = 0.7325$. Repeated analyses of Nd (JNdi-1) and Hf (in-house solution) standard solutions gave $^{143}Nd/^{144}Nd$ of 0.512117 ± 0.000012 (2 SD, n = 16), and $^{176}Hf/^{177}Hf$ of 0.282154 ± 0.000009 (2 SD, n = 11), corresponding to an external reproducibility (2 SD) of ± 0.23ε_{Nd} and ± 0.31ε_{Hf}, respectively. Epsilon Nd and Hf values were calculated using $^{143}Nd/^{144}Nd = 0.512630$ and $^{176}Hf/^{177}Hf = 0.282785$ (Bouvier et al., 2008). The measured Nd and Hf isotopic ratios were used to calculate the $\Delta\varepsilon_{Hf\ clay}$ index, which corresponds to the deviation of Hf isotopic compositions from the Clay Array ($\varepsilon_{Hf} = 0.78 \times \varepsilon_{Nd} + 5.23$) in the ε_{Hf} versus ε_{Nd} diagram (Bayon et al., 2016).

2.5. Core chronology

^{210}Pb and ^{226}Ra activities were measured in core MOZ1-MTB-7 using gamma spectrometry on dried sediment with a well-type high efficiency low background germanium detector (CANBERRA) equipped with a Cryo-Cycle (Table 4). Calibration of the gamma spectrometer was established using IAEA-RGU-1 reference material. $^{210}Pb_{xs}$ was determined by taking the difference between the measured activities of ^{210}Pb and its parent ^{226}Ra. To generate the age-depth model, we applied two models: the CF-CS (constant flux-constant sedimentation) model and the CIC (constant initial concentration) model. Additional chronological constraints were provided by ^{14}C ages on bulk planktonic foraminifera taken from the lower part of core MOZ1-MTB7 (n = 2) and from nearby core MOZ1-KSF10 (n = 11) (Table 5). They were first corrected for a reservoir age of 426 ± 76 ^{14}C years and then calibrated to calendar age using the IntCal13 calibration curve (Southon et al., 2002; Reimer et al., 2013; Soulet, 2015). The final age model for core MOZ1-KSF-10 was performed using the "classical" (non-bayesian) age modeling software Clam (Blaauw, 2010). Calculations were performed at 95% confidence. Temporal clamping between both cores MOZ1-MTB-6 and MOZ1-MTB-7 was based on calcium carbonate content and Ca elemental composition respectively. Note that there is a gap in the temporal data between ~ 1000 and ~ 3500 years BP due to that section of core MOZ1-KSF-10 being lost during piston coring.

Table 3
Neodymium and Hafnium isotopic measurements in core MOZ1-MTB-7.

MOZ1-MTB-7					
Sediment interval (cm)	**εNd**	**Error (2σ)**	**εHf**	**Error (2σ)**	**$\Delta\varepsilon_{Hf\ clay}$**
0–1	− 19.32	0.13	− 2.36	0.22	7.5
2–3	− 19.30	0.11	− 2.22	0.18	7.6
4–5	− 20.11	0.10	− 2.89	0.21	7.6
6.5–7	− 19.52	0.10	− 2.94	0.18	7.1
9–9.5	− 19.19	0.11	− 2.90	0.28	6.8
10–10.5	− 19.57	0.11	− 3.85	0.22	6.2
12–12.5	− 19.66	0.11	− 3.81	0.19	6.3
13–13.5	− 19.77	0.10	− 4.32	0.19	5.9
14–15	− 19.95	0.09	− 3.95	0.16	6.4
21–22	− 19.54	0.11	− 5.03	0.14	5.0
29–30	− 19.20	0.08	− 5.10	0.15	4.6
35–36	− 19.35	0.10	− 5.43	0.23	4.4
45–46	− 18.89	0.08	− 6.17	0.29	3.3
47–48	− 19.09	0.09	− 5.67	0.19	4.0

Table 4
Total ^{210}Pb radionuclide activity and related ages in core MOZ1-MTB-7.

MOZ1-MTB-7					
Sediment interval	**$^{210}Pb_{xs}$**		**Age**		**Age**
cm	**mBq/g**	**±**	**CF-CS model**	**±**	**CIC**
0–1	1372	28	2013	0.3	2015
1–2			2009	0.9	
2–3	118	12	2005	1.5	1936
3–4	631	9	2001	2.1	1990
4–5			1997	2.7	
5–6	1046	17	1993	3.3	2006
6–7			1989	3.9	
7–8	290	12	1985	4.5	1965
8–9			1981	5.1	
9–10	303	25	1977	5.7	1966
10–11	243	9	1973	6.3	1959
11–12			1969	6.9	
12–13	358	12	1965	7.5	1972
13–14	38	4	1961	8.1	1899
14–15	5	4	1957	8.7	1834
15–16	211	10	1953	9.4	1955
16–17	121	8	1935	12.0	1937
17–18	39	3	1918	14.6	1900
18–19	8	4	1900	17.2	1848
19–20			1883	19.8	
20–21	13	4	1866	22.4	1864
25–26	1	3	*1779*	*35.5*	*1776*
30–31	− 4	2			

2.6. Benthic foraminifera

Fossil benthic foraminifera (> 125 μm) were investigated in 11 sediment intervals from core MOZ1-MTB-7. For each sediment interval, a mean volume of 18 cc was sieved through both 63 and 125 μm mesh screens and then dried in an oven (50 °C). Sediment residues (> 125 μm) were split in aliquots using an Otto micro-splitter to get at least 200 benthic foraminiferal specimens per sediment interval. Foraminifera were hand-picked and stored in Plummer slides, counted and identified using holotype descriptions inventoried in the Ellis and Messina catalogue (1940 et seq.) (Appendix A). In each sediment interval, we determined foraminiferal density (ind./50 cc), the relative abundances of each species, the Berger-Parker index (i.e. highest specific percentage per interval), species richness S, and Shannon index H′. Species richness S represents the number of taxa per interval and Shannon index H′ is sensitive to S but also indicates the relative

Table 5
^{14}C-AMS dates used for the chronology of MOZ1-MTB-7 and MOZ1-KSF-10.

Core label	Depth (cm)	Lab. number	Species	^{14}C age (yr BP)	Error (1σ)	Reservoir correction[a] (^{14}C yr)	Error[a] (1σ)	^{14}C age corrected for reservoir[b] (^{14}C yr BP)	Error[c] (1σ)	Calendar age range[d] (yr BP, 2σ)
MOZ1-MTB-7	37	Beta-440164	bulk planktonic foraminifera	1250	30	426	76	824	82	659–922
MOZ1-MTB-7	49	Beta-411043	bulk planktonic foraminifera	1440	30	426	76	1014	82	734–1086
MOZ1-KSF-10	0	Beta-413670	bulk planktonic foraminifera	3820	30	426	76	3394	82	3451–3845
MOZ1-KSF-10	70	Beta-433011	bulk planktonic foraminifera	3730	30	426	76	3304	82	3363–3721
MOZ1-KSF-10	280	Beta-413671	bulk planktonic foraminifera	8170	30	426	76	7744	82	8381–8725
MOZ1-KSF-10	400	Beta-413672	bulk planktonic foraminifera	9900	30	426	76	9474	82	10,544–11,095
MOZ1-KSF-10	440	Beta-433009	bulk planktonic foraminifera	9930	40	426	76	9504	86	10,571–11,132
MOZ1-KSF-10	530	Beta-433010	bulk planktonic foraminifera	11,360	40	426	76	10,934	86	12,699–13,007
MOZ1-KSF-10	630	Beta−413673	bulk planktonic foraminifera	12,700	40	426	76	12,274	86	13954–14,722
MOZ1-KSF-10	680	Beta-433008	bulk planktonic foraminifera	13,530	50	426	76	13,104	91	15,357–16,011
MOZ1-KSF-10	780	Beta-433007	bulk planktonic foraminifera	14,360	50	426	76	13,934	91	16,540–17,206
MOZ1-KSF-10	890	Beta-433012	bulk planktonic foraminifera	15,720	50	426	76	15,294	91	18,337–18,753
MOZ1-KSF-10	930	Beta-421623	bulk planktonic foraminifera	15,690	50	426	76	15,264	91	18,317–18,740
MOZ1-KSF-10	940	Beta-421624	bulk planktonic foraminifera	16,250	60	426	76	15,824	97	18,859–19,377

[a] Reservoir correction in Southon et al. (2002) and Soulet (2015).
[b] Corrected ^{14}C ages are obtained by subtracting the reservoir correction to the original ^{14}C age.
[c] Errors associated to the corrected ^{14}C were propagated through the quadratic sum.
[d] Corrected ^{14}C ages were then calibrated using the atmospheric calibration curve IntCal13 in Reimer et al. (2013).

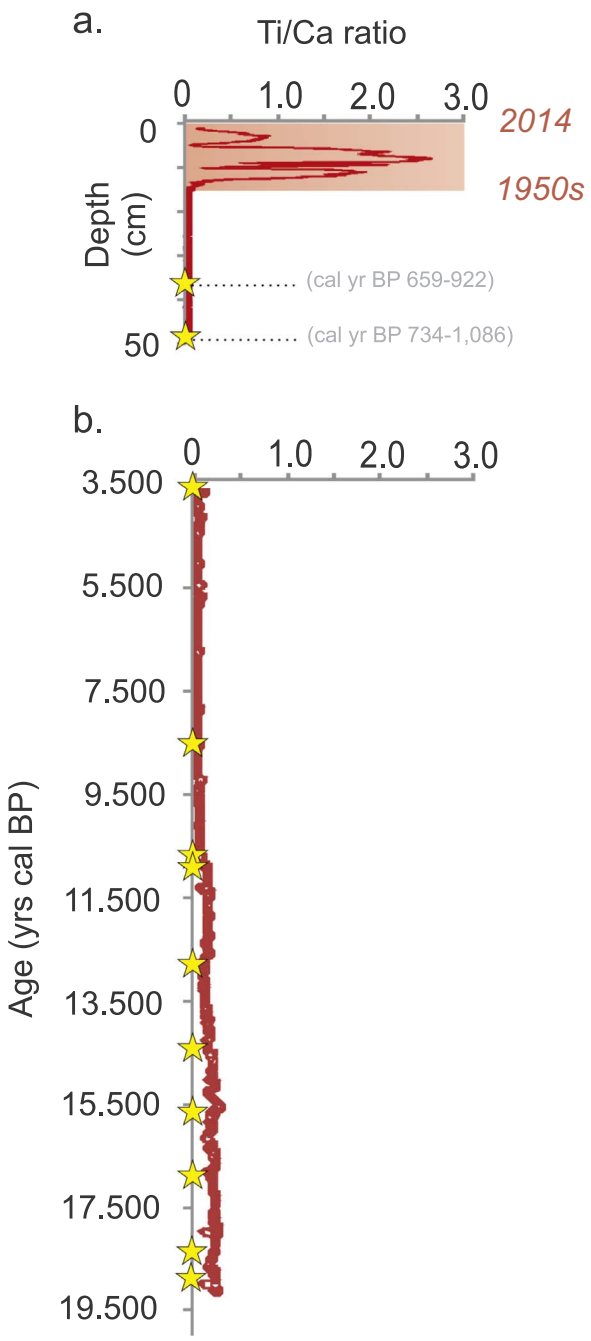

Fig. 3. Historical record versus Pleistocene-Holocene transition period. Ti/Ca ratio recorded in core MOZ-MTB-7 (depth expressed in cm below the sediment-water interface) (**a**) and in core MOZ-KSF-10 (depth expressed in calendar age BP) (**b**). Radiocarbon ages in both archives are indicated by yellow stars. Pale red band indicates sediments deposited since the 1950s. (For interpretation of the references to color in this figure legend, the reader is referred to the web version of this article.)

contribution of all taxa (Murray, 2006).

3. Results and discussion

The uppermost 15 cm of core MOZ1-MTB-7 is characterized by three successive layers of fine-grained sediments depleted in calcium (Ca) and enriched in titanium (Ti), inherited from strongly weathered lateritic soils (Berger et al., 2014). These silt-clay sediments contrast with the more homogeneous and slightly coarser hemipelagic material encountered in the lower 35 cm (Fig. 2). Depth profiles of excess ^{210}Pb and ^{14}C dates also illustrate that the uppermost ~ 15 cm corresponds to a drastic change in sedimentation rates (Fig. 2). Sediments from the base of the core (i.e. ca 1000 years ago) up to 15 cm (i.e. 1950s) accumulated at a mean sedimentation rate of 0.4 mm/year, whilst the uppermost Ti-rich sediments were deposited with a mean sedimentation rate of 2.5 mm/year, six times greater than the underlying sediments. When compared to the Late Quaternary record provided by core MOZ1-KSF10 (Fig. 3), the Ti/Ca profile measured for the MTB cores departs significantly from the natural Ti/Ca pattern of the last twenty millenia. This observation suggests that modern source-to-sink connections between land and the deep-sea, and associated sediment transfer, is completely unlike the natural sedimentation pattern that has prevailed in this region for the last 20,000 years.

From 15 to 0 cm in core MOZ1-MTB-7, the increasing $\Delta\varepsilon_{Hf\ clay}$ values, considered a new proxy for silicate weathering intensity (Bayon et al., 2012), indicates a stronger degree of soil alteration, consistent with soils that have undergone a deforestation event. The absence of any significant change in Nd isotopic ratios (ε_{Nd}) suggests that most of the sediment delivered to the study site pre- and post-1950s derives from a similar source region, likely both the Mahavavy Sud and Betsiboka drainage areas (Fig. 2) (Bayon et al., 2016). Interestingly, terrigenous material deposited after the 1950s is accompanied by the enhanced burial of organic compounds (OC content > 2% Dry Weight), characterized by relatively uniform C/N signatures (values between 9 and 11) similar to those documented in other sub-tropical intertidal mangroves (Fig. 2) (Ralison et al., 2008). The increase of chlorophyll b (Chl *b*), which is mainly related to land plants, demonstrates preferential contribution from terrestrial organic material rather than marine compounds in the depositional layers covering the last 60 years (Fig. 2). This correlates with the overall freshness of chlorophyll phytopigments (Chl *a* and Chl *b* compared to phaeopigments *a* and *b*), which increase in organic-carbon-enriched intervals, further suggesting a rapid transfer to the deep seafloor. The minor increase in the C/N ratio after the 1950s could be related to the preferential preservation of terrestrial organic nitrogen compounds when they are adsorbed by clay minerals (Müller, 1977).

Observations recorded here suggest a significant increase in soil erosion in northwestern Madagascar since 1950s, delivering pulses of substantial terrestrial material from multiple catchments to the seafloor. Whilst human-induced changes in land-use and vegetation cover constitute a questionable catalyst for the abrupt alteration of the studied benthic environment since the 1950s, the increasing intensity of tropical cyclones (TCs) within the south-west Indian Ocean may account for the observed environmental degradation (Emanuel, 2005; Webster et al., 2005; Elsner et al., 2008; Knutson et al., 2010). Madagascar is located along the tropical cyclone track of the southern hemisphere (Fitchett and Grab, 2014; Mavume et al., 2009). In recent decades, tropical cyclone intensity in this region has increased, likely in relation to the southern Indian Ocean's warming sea surface temperature (Webster et al., 2005; Elsner et al., 2008). This has lead to an increase in the frequency of erosional storm surges over NW Madagascar. In February and March 1959, an exceptional series of tropical cyclones caused torrential rainfall and catastrophic floods, triggering tremendous landslides and intense erosion from deforested areas and fallow lands (Saboureau, 1959). At that time, the disaster was considered unique in Madagascan history (Saboureau, 1959). In February 1972, Cyclone Eugénie generated substantial floods in Betsiboka and Mahavavy Sud catchment basins. More recently (March 2004), Cyclone Gafilo, a category-5 TC on the Saffir-Simpson-Hurricane Wind Scale, also struck Madagascar causing catastrophic devastation on land. It is considered the most intense modern cyclone ever recorded in the south-west Indian Ocean. These three remarkable cyclonic events may have resulted in three major gravity-flows recorded in our sedimentary record since the 1950s (i.e., three successive layers of sediments enriched in Ti). For the last century, it is possible that the current global warming trend has induced a gradual increase in the frequency of erosional storm surges associated with highly destructive TCs over NW Madagascar.

Unfortunately, historical archives prior to the mid-20th century are too sparse and imprecise to provide a coherent record of TC frequency and strength over the last century and millenia. Alternatively Madagascar has been experiencing ongoing tectonic uplift since the Cenozoic, resulting in deep incisions of continental crust by rivers (Stephenson and White, 2016). The distribution of major erosional gullies (i.e., lavakas) are uneven, and focused in the central highlands where seismic activity is recorded (Cox et al., 2010). Therefore, both the Mahavavy Sud and Betsiboka rivers, which drain the central highlands, may efficiently transfer lateritic material from pre-existing lavakas to the NW Madagascan margin (our study area). It is possible a major seismic event affecting NW Madagascar in the 1950s provoked enhanced soil erosion in the central highlands around preexisting structural faults, followed by a massive transportation of terrestrial material by rivers to marine shelves during torrential rains. Such an earthquake, if proved to exist, could have modified coastal topography around the river mouths (e.g., channel avulsion), accompanied by a straightforward connection between the Mahavavy Sud and Betsiboka rivers and our study area (deep-sea interfluve). We recovered only a few qualitative sources of information regarding seismic activity in NW Madagascar (Terrier et al., 2000), inhibiting the possibility to directly connect seismicity and sedimentary input in our study area.

Regardless, the abrupt change in observed sedimentation patterns after the 1950s is accompanied by a major ecological shift in microfaunal composition and diversity at the seafloor. The foraminiferal content in the last 60 years is much lower (< 800 ind./50 cc above 11 cm depth) compared to older sediments where dead foraminiferal tests are relatively abundant (> 5000 ind./50 cc below 19 cm depth) (Fig. 4). This depletion is partly related to the abrupt increase of sedimentation rates and a correlative dilution effect. However *Bulimina marginata,* an opportunistic species able to recolonize ecosystems with recurrent sediment instability (Hess and Jorissen, 2009; Fontanier et al., 2012), dominates the foraminiferal assemblages after the 1950s (Fig. 4). This faunal change coincides with a drop in diversity, as inferred from the lower Shannon index H′ and species richness S values in the most recent decades (Fig. 4). Not only has the deep-sea sedimentary budget drastically changed quantitatively and qualitatively, but the benthic ecosystems, exemplified by deep-sea foraminifera, have responded to recurrent stress with lowered diversity and dominance by an opportunistic taxon.

In the light of our highly multidisciplinary study, we conclude that the seafloor off NW Madagascar has been repeatedly disturbed by the deposition of organic rich, tropical, terrestrial sediments for the last 60 years. This abrupt sedimentary change has caused marked reductions in benthic foraminiferal biodiversity. Increased soil erosion due to local land-use, deforestation and intensifying tropical cyclones are potential causes for the sedimentary budget and biodiversity shift. Our interpretations, which are based on only one sampling area (i.e. an interfluve between two submarine canyons), are still tentative. Further studies of modern sedimentary records recovered from other submarine

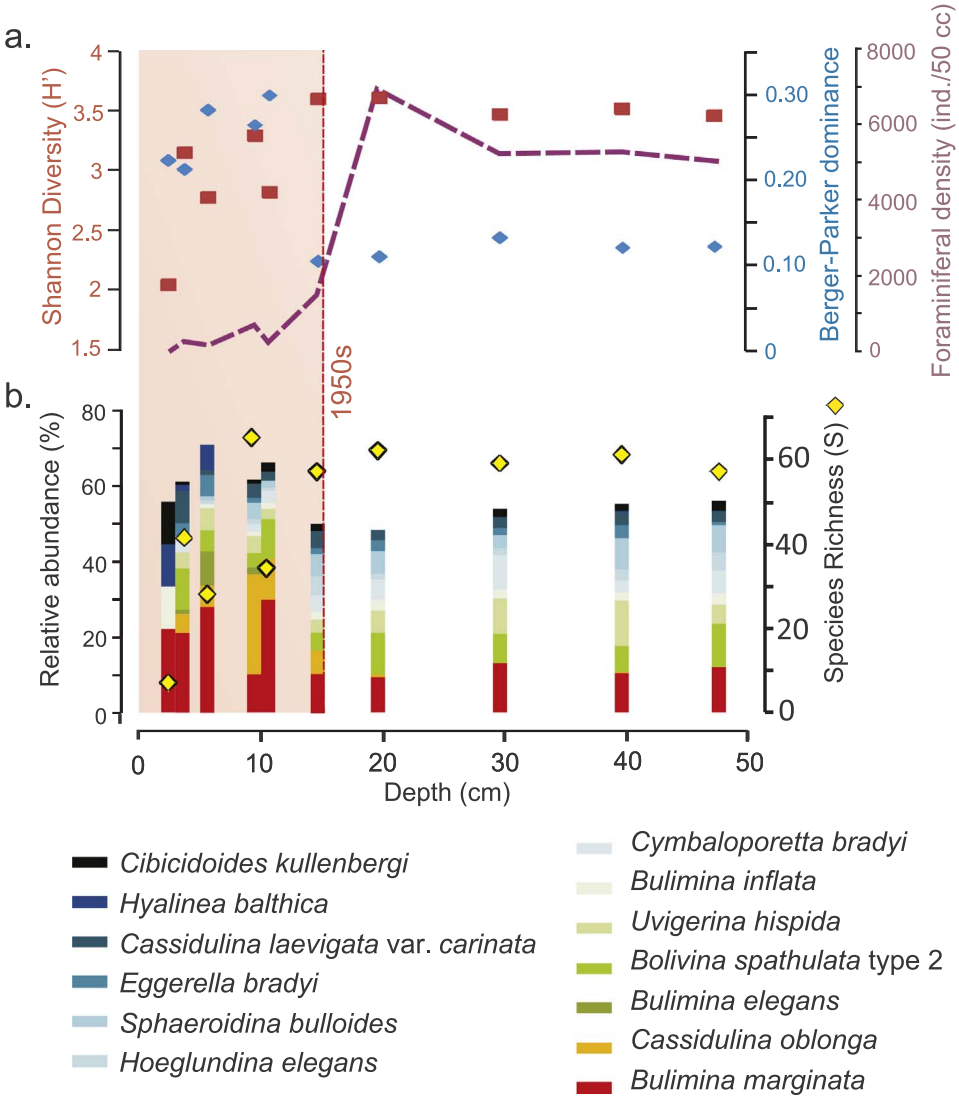

Fig. 4. Alteration of benthic diversity since the 1950s a: Shannon diversity (H′), Berger-Parker Dominance and Foraminiferal density (ind./50 cc) in core MOZ1-MTB-7. **B:** Composition of fossil foraminiferal fauna expressed in relative abundance (in %) in core MOZ1-MTB-7. Only major species (> 5%) are pictured. Species Richness (S) is also pictured. Pale red band indicates sediments deposited since the 1950s.

canyon systems from NW Madagascar are necessary in order to better constrain the temporal variability of source-to-sink connections between the land and deep-sea during the last two centuries.

Acknowledgements

This study was done in the framework of the PAMELA project ("Passive Margin Exploration Laboratories") funded by TOTAL and Ifremer. We thank crew members of the R/V *L'Atalante,* K. Olu (chief scientist) and all scientists who participated to the PTOLEMEE and PAMELA-MOZ1 cruises. We thank crew members of the International Space Station for providing high-quality photographs from the Betsiboka area. Eline Garnier's fellowship was funded by the ECOBIOC Team from the laboratory "Environnements et Paléo-environnements Océaniques et Continentaux" (UMR 5805), University of Bordeaux. E. Ponzevera is thanked for help during MC-ICPMS analyses. We thank two reviewers and associate editors for their helpful comments on the manuscript.

Authors contribution

C.F. designed the study, performed foraminiferal and sedimentological work and wrote the manuscript. R.L.M. and P.D. conducted work on benthic foraminiferal faunas. S.S. performed radionuclide (210Pb) measurements. S.T., A.B. and S.C. performed core scanner XRF measurements. A.R., D.B., E.G. and S.B. were in charge of grain-size analyses. G.B. analysed Hf and Nd isotopic compositions. D.B., M.R., A.R., and C.F. scanned and photographed the sediment cores. B.D., E.G., S.B. and A.G. performed sedimentary organic matter. S.S. and T.T. provided isotopic data on benthic foraminifera. G.J. and S.D. interpreted the sedimentary context of this study area and were involved in the geophysical data acquisition and interpretation to better assess the pertinence of the selected sampling sites. M.P and A.S. prepared Fig. 1. S.J. and K.O. were scientist coordinators during the 2014 PTOLEMEE and PAMELA-MOZ1 cruises, respectively. B.M. revised the English of the draft and provided constructive comments to improve the understanding of our story. All authors participated to data interpretation and provided comments on the manuscript.

Appendix A. Supplementary material

Supplementary data associated with this article can be found in the online version at http://dx.doi.org/10.1016/j.dsr.2017.11.011.

References

Bayon, G., Denniellou, B., Etoubleau, J., Ponzevera, E., Toucanne, S., Bermell, S., 2012. Intensifying weathering and land use in iron age Central Africa. Science 335, 1219–1222.

Bayon, G., Skonieczny, C., Delvigne, C., Toucanne, S., Bermell, S., Ponzevera, E., André, L., 2016. Environmental Hf-Nd isotopic decoupling in World river clays. Earth Planet. Sci. Lett. 438, 25–36.

Berger, A., Janots, E., Gnos, E., Frei, R., Bernier, F., 2014. Rare earth element mineralogy and geochemistry in a laterite profile from Madagascar. Appl. Geochem. 41, 218–228.

Blaauw, M., 2010. Methods and code for 'classical' age-modelling of radiocarbon sequences. Quat. Geochronol. 5, 512–518.

Bouvier, A., Vervoort, J.D., Patchett, P.J., 2008. The Lu–Hf and Sm–Nd isotopic composition of CHUR: constraints from unequilibrated chondrites and implications for the bulk composition of terrestrial planets. Earth Planet. Sci. Lett. 273, 48–57.

Cox, R., Zentner, D.B., Rakotondrazafy, A.F.M., Rasoazanamparany, C.F., 2010. Shakedown in Madagascar: occurrence of lavakas (erosional gullies) associated with seismic activity. Geology 38 (2), 179–182.

Ellis, B.F., Messina, A.R., 1940. The Brooks F. Ellis and Angelina R. Messina Catalogue of Foraminifera. American museum of natural history, New York.

Elsner, J.B., Kossin, J.P., Jagger, T.H., 2008. The increasing intensity of the strongest tropical cyclones. Nature 455, 92–95.

Emanuel, K., 2005. Increasing destructiveness of tropical cyclones over the past 30 years. Nature 436, 686–688.

Fitchett, J.M., Grab, S.W., 2014. A 66-year tropical cyclone record or south-east Africa: tropical trends in a global context. Int. J. Climatol. http://dx.doi.org/10.1002/joc.3932.

Fontanier, C., Fabri, M.-C., Buscail, R., Biscara, L., Koho, K., Reichart, G.J., Cossa, D., Galaup, S., Chabaud, G., Pigot, L., 2012. Deep-sea foraminifera from the Cassidaigne Canyon (NW Mediterranean): assessing the environmental impact of bauxite red mud disposal. Mar. Pollut. Bull. 64, 1895–1910.

Fontanier, C., Garnier, E., Brandilly, C., Dennielou, B., Bichon, S., Gayet, N., Eugene, T., Rovere, M., Grémare, A., Deflandre, B., 2016. Living (stained) benthic foraminifera from the Mozambique Channel (eastern Africa): exploring ecology of deep-sea unicellular meiofauna. Deep-Sea Res. Part-I. http://dx.doi.org/10.1016/j.dsr.2016.06.007.

Gade, D.W., 1996. Deforestation and its effects in highland Madagascar. Mt. Res. Dev. 16, 101–116.

Green, G.M., Sussman, R.W., 1990. Deforestation history of the eastern rain forests of Madagascar from satellite images. Science 248, 212–215.

Grove, C.A., Zinke, J., Peeters, F., Park, W., Scheufen, T., Kasper, S., Randriamanantsoa, B., McCulloch, M.T., Brummer, G.J.A., 2013. Madagascar corals reveal multidecadal modulation of rainfall since 1708. Clim. Past. 9, 641–656.

Harper, G.J., Steininger, M.K., Tucker, C.J., Juhn, D., Hawkins, F., 2007. Fifty years of deforestation and forest fragmentation in Madagascar. Environ. Conserv. 34 (4), 325–333.

Helfert, M.R., Wood, C.A., 1986. Shuttle photos show Madagascar erosion. Geotimes 31, 4–5.

Hess, S., Jorissen, F.J., 2009. Distribution patterns of living benthic foraminifera from Cap Breton canyon, Bay of Biscay: faunal response to sediment instability. Deep-Sea Res. Part-I 56, 1555–1578.

Jarosz, L., 1993. Defining and explaining tropical deforestation: shifting cultivation and population-growth in colonial Madagascar (1896–1940). Econ. Geogr. 69 (4), 366–379.

Jorry, S.J., 2014. ⟨http://dx.doi.org/10.17600/14000900⟩.

Klein, J., 2002. Deforestation in the Madagascar Highlands – established 'truth' and scientific uncertainty. GeoJournal 56, 191–199.

Knutson, T.R., McBride, J.L., Chan, J., Emanuel, K., Holland, G., Landsea, C., Held, I., Kossin, J.P., Srivastava, A.K., Sugi, M., 2010. Tropical cyclones and climate change. Nat. Geosci. 3 (3), 157–163.

Kull, C.A., 2000. Deforestation, erosion, and fire: degradation myths in the environmental history of Madagascar. Environ. Hist. 6 (4), 423–450.

Maina, J., de Moel, H., Zinke, J., Madin, J., McClanahan, T., Vermaat, J.E., 2013. Human deforestation outweighs future climate change impacts of sedimentation on coral reefs. Nat. Commun. 4, 1986. http://dx.doi.org/10.1039/ncomms2986.

Mavume, A.F., Rydberg, K., Rouault, M., Lutjeharms, J.R.E., 2009. Climatology and landfall of tropical cyclones in the South-West Indian Ocean. West Indian J. Mar. Sci. 8 (1), 15–36.

Müller, P.J., 1977. C/N ratios in Pacific deep-sea sediments: effect of inorganic ammonium and organic nitrogen compounds sorbed by clays. Geochim. Cosmochim. Acta 41, 765–776.

Murray, J.W., 2006. Ecology and Applications of Benthic Foraminifera. Cambridge University Press, Cambridge, pp. 426.

Myers, M., Mittermeier, R.A., Mittermeier, C.G., da Fonseca, G.A.B., Kent, J., 2000. Biodiversity hotspots for conservation priorities. Nature 403, 853–858.

Neveux, J., Lantoine, F., 1993. Spectrofluorometric assay of chlorophylls and phaeopigments using the least squares approximation technique. Deep-Sea Res. I 40 (9), 1747–1765.

Olu, K., 2014. ⟨http://dx.doi.org/10.17600/14001000⟩.

Pastor, L., Deflandre, B., Viollier, E., Cathalot, C., Metzger, E., Rabouille, C., Escoubeyrou, K., Lloret, E., Pruski, A.M., Vétion, G., Desmalades, M., Buscail, R., Grémare, A., 2011. Influence of the organic matter composition on benthic oxygen demand in the Rhône River prodelta (NW Mediterranean Sea). Cont. Shelf Res. 31, 1008–1019.

Ralison, O.H., Borges, A.V., Dehairs, F., Middelburg, J.J., Bouillon, S., 2008. Carbon biogeochemistry of the Betsiboka estuary (north-western Madagascar). Org. Geochem. 39, 1649–1658.

Reimer, P.J., Bard, E., Bayliss, A., Beck, J.W., Blackwell, P.G., Ramsey, C.B., Buck, C.E., Cheng, H., Edwards, R.L., Friedrich, M., Grootes, P.M., Haflidason, H., Hajdas, I., Hatté, C., Heaton, T.J., Hoffmann, D.L., Hogg, A.G., Hughen, K.A., Kaiser, K.F., Kromer, B., Manning, S.W., Niu, M., Reimer, R.W., Richards, D.A., Scott, E.M., Southon, J.R., Staff, R.A., Turney, C.S.M., van der Plicht, J., 2013. IntCal13 and Marine13 radiocarbon age calibration curves 0–50,000 years cal BP. Radiocarbon 55 (4), 1869–1887.

Saboureau, P., 1959. Propos sur les cyclones et inondations à Madagascar en février et mars 1959. Rev. Bois For. Des. Trop. 67, 3–12.

Soulet, G., 2015. Methods and codes for reservoir–atmosphere ^{14}C age offset calculations. Quat. Geochronol. 29, 97–103.

Southon, J., Kashgarian, M., Fontugne, M., Metivier, B., Yim, W.W.S., 2002. Marine reservoir corrections for the Indian Ocean and Southeast Asia. Radiocarbon 44 (1), 167–180.

Stephenson, S., White, N., 2016. Cenozoik uplift, erosion and dynamic support of Madagascar. Geophys. Res. Abstr. 18 (EGU General Assembly 2016, EGU2016-11009-2).

Terrier, M., Audru, J.-C., Bour, M., Dominique, P., 2000. Etude de l'alée sismique régional de l'île de Mayotte; détermination des mouvements sismiques de référence. Rapp. BRGM RP-50250-FR 95.

Waeber, P.O., Wilmé, L., Ramamonjisoa, B., Garcia, C., Rakotomalala, D., Rabemananjara, Z.H., Kull, C.A., Ganzhorn, J.U., Sorg, J.-P., 2015. Dry forests in Madagascar: neglected and under pressure. Int. For. Rev. 17 (S2), 127–148.

Webster, P.J., Holland, G.J., Curry, J.A., Chang, H.R., 2005. Changes in tropical number, duration and intensity in a warming environment. Science 309, 1844–1846.